Shocks and dust formation in Nova V809 Cep

Aliya-Nur Babul,[1]★ Jennifer L. Sokoloski,[1] Laura Chomiuk,[2] Justin D. Linford,[3] Jennifer H.S. Weston,[4] Elias Aydi,[2] Kirill V. Sokolovsky [2,5] Adam M. Kawash [2]

[1]Department of Astronomy, Columbia University, 550 W 120th St, New York, NY 10027, USA
[2]Center for Data Intensive and Time Domain Astronomy, Department of Physics and Astronomy, Michigan State University, East Lansing, MI 48824, USA
[3]National Radio Astronomy Observatory, P.O. Box O, Socorro, NM 87801, USA
[4] Federated IT, 1201 Wilson Blvd, 27th Floor, Arlington VA 22209
[5] Sternberg Astronomical Institute, Moscow State University, Universitetskii pr. 13, 119992 Moscow, Russia

3 March 2022

arXiv:2106.15782v1 [astro-ph.HE] 30 Jun 2021

ABSTRACT

The discovery that many classical novae produce detectable GeV γ-ray emission has raised the question of the role of shocks in nova eruptions. Here we use radio observations of nova V809 Cep (Nova Cep 2013) with the Jansky Very Large Array to show that it produced non-thermal emission indicative of particle acceleration in strong shocks for more than a month starting about six weeks into the eruption, quasi-simultaneous with the production of dust. Broadly speaking, the radio emission at late times – more than a six months or so into the eruption – is consistent with thermal emission from 10^{-4} $M_\odot$ of freely expanding, 10^4 K ejecta. At 4.6 and 7.4 GHz, however, the radio light-curves display an initial early-time peak 76 days after the discovery of the eruption in the optical (t_0). The brightness temperature at 4.6 GHz on day 76 was greater than $10^5 K$, an order of magnitude above what is expected for thermal emission. We argue that the brightness temperature is the result of synchrotron emission due to internal shocks within the ejecta. The evolution of the radio spectrum was consistent with synchrotron emission that peaked at high frequencies before low frequencies, suggesting that the synchrotron from the shock was initially subject to free-free absorption by optically thick ionized material in front of the shock. Dust formation began around day 37, and we suggest that internal shocks in the ejecta were established prior to dust formation and caused the nucleation of dust.

1 INTRODUCTION

A classical nova is an eruption that occurs in an interacting stellar binary system in which one star is a white dwarf and the other is typically a main sequence star (Chomiuk et al. 2020a; Della Valle & Izzo 2020). Hydrogen-rich material from the donor star accretes onto the white dwarf and is compressed, causing the temperature to rise. The soaring temperatures trigger a thermonuclear runaway and a subsequent ejection of matter from the white dwarf (Starrfield et al. 2016). As material is ejected from the white dwarf, the system brightens across much of the electromagnetic spectrum, allowing for the discovery of such phenomenon.

Between its launch in 2008 June and 2021 April, the Large Area Telescope (LAT; Atwood et al. 2009) of the *Fermi Gamma Ray Space Telescope* detected GeV gamma-rays from 17 novae (see the list in Chomiuk et al. 2020b; Franckowiak et al. 2018, plus the recurrent nova V3890 Sgr; Buson et al. 2019), typically within a few days of their optical peak (e.g., Ackermann et al. 2014; Chomiuk et al. 2020a,b) The presence of GeV gamma-rays implies that these eruptions have generated a population of relativistic particles. These particles are likely produced via the diffusive shock acceleration mechanism as a result of internal shocks within the ejecta (e.g., Blandford 1994; Metzger et al. 2016). The high-energy particles may produce gamma-rays via a number of processes including pion decay, inverse Compton scattering of ambient optical photons and relativistic bremsstrahlung (Metzger et al. 2015; Martin et al. 2018). High-energy particles may also produce synchrotron radiation in the radio band (Vlasov et al. 2016). Radio imaging of nova V959 Mon revealed regions of synchrotron emission, further confirming the presence of shocks and providing a localization within the ejecta. From the images, Chomiuk et al. (2014a) postulated that the shocks are the result of collisions between two outflows from the white dwarf: the first, more slowly moving outflow having a toroidal geometry, and the second, faster flow having a more spherical geometry. The shocks were located near the equatorial plane, where the two outflows collided. Based on the optical spectral evolution of a large sample of novae, Aydi et al. (2020b) found consistent evidence for this colliding outflows scenario Finally, observations of correlated variations in GeV and optical brightness suggest that shocks may transport a significant fraction of the nova eruption energy (Li et al. 2017; Aydi et al. 2020a) and power a substantial fraction of the bolometric luminosity during the early weeks of a nova eruption.

In nova-producing binaries that are too distant for γ-ray detections, radio observations provide a unique opportunity to study developing shocks. Radio lightcurves sometimes contain local maxima, which we refer to as *early-time flares*, within months of the initial optical peak (Taylor et al. 1987; Finzell et al. 2018; Weston et al. 2016a). These early-time flares correspond to radio surface brightnesses (parameterized as brightness temperatures) that are at least an order of magnitude higher than expected from thermally emitting, 10^4 K ionized gas that is expanding freely with speeds inferred from optical spectral lines (Cunningham et al. 2015). Because the brightness temperature represents a lower limit on the temperature of thermally emitting material, brightness temperatures in excess of 10^5 K indicate that either the the ejecta contain enough T $\geqslant$ 10^5 K gas for that gas to be optically thick to free-free emission at radio wavelengths or the radio emission is non-thermal emission from electrons accelerated via shocks. In at least one case (V1723 Aql), Weston et al. (2016a) argued that the mass of 10^5 K gas required for the ejecta to generate the observed radio emission through thermal

© 2018 The Authors

processes was unfeasible, and that the high brightness temperature was more likely to be the result of synchrotron emission produced near the internal shocks in the ejecta (Vlasov et al. 2016).

Optical and Infared (IR) light curves of classical novae sometimes display characteristics of dust formation days to months after the initial eruption (e.g., Evans 2001; Shore et al. 2018). Sudden decreases in the optical flux are seen in about 20 percent of novae within 100 days of the optical peak (Strope et al. 2010). These decreases occur earlier than what would be expected due to the natural fading in nova luminosity over time, and – along with the subsequent optical rebrightenings – are referred to as "dust dips". They result from the obscuring of some optical light from the nova due to the formation of dust and also often appear along with brightening at infrared wavelengths, a typical signature of dust emission (Gehrz 2008).

Dust production requires cool ($T \lesssim 10^3$ K) gas for the condensation of dust grains, and regions of dust condensation must be shielded from the ionizing radiation emanating from the white dwarf. Derdzinski et al. (2017); Gallagher (1977) reconciles the presence of harsh radiation with the onset of dust formation. Their model, which we refer to as the *Shock-Dust Model*, postulates that dense radiative shocks, such as the ones thought to give rise to the γ-rays and early-time radio peaks, provide the optimal conditions for dust condensation. As both the forward and reverse shocks progress, the gas density behind the shocks increases rapidly, producing a thin shell of dense gas between the forward and reverse shocks (Steinberg & Metzger 2018; Vlasov et al. 2016). This shell is dense enough to be protected from radiation, and as the gas cools, molecules can begin to nucleate into dust particles. Because radio imaging shows that shocks are produced at the interface between the slow-moving toroidal outflow and the fast-moving spherical outflow, the dense shells (and dust formation) might be localized in the equatorial plane.

V809 Cep was first discovered in a nova eruption on 2013 February 2 by K. Nishiyama and F. Kabashima (CBET 3397), and we take this date to be the start of the eruption, t_0. V809 Cep reached peak optical brightness one day later (Munari et al. 2014). Emission line profiles on day 220 and 352 for [OIII] 5007 Å and [NII] 6548, 6584 + Hα had a double peak with a separation of 1160 km/s corresponding to a bulk velocity of 600 km/s (Munari et al. 2014). Using the Echelle spectra and comparing with Brand & Blitz (1993), Munari et al. (2014) found the lower limit on the distance to be 6 kpc associated with the crossing of the Perseus or Outer arm. Additionally, using methods from Downes & Duerbeck (2000) and MMRD techniques, they refined their distance estimate to 6.5 kpc. We thus take the distance to be D=6.5 kpc.

In this paper, we use radio observations to show that nova V809 Cep produced non-thermal emission quasi-simultaneously with dust production. We postulate that the non-thermal emission occurred prior to the dust formation, but was initially absorbed by photo-ionized gas ahead of the shock. In Section 2, we describe the technical details of the observations and data reduction. In Section 3, we present our results, and in Section 4 we discuss the implications of our findings in validating the shock-dust model.

2 OBSERVATIONS

We monitored V809 Cep using the Karl G. Jansky Very Large Array Telescope (VLA) between 2013 February 14 and 2016 January 28 under programs 13A-455, 13B-057, and 15B-343. Between 2013 February and 2016 January, the VLA cycled through all configurations, and observed V809 Cep at C band (4 – 8 GHz), Ku band (12 – 18 GHz), and Ka band (26 – 40 GHz). All the observations from 2013 February to 2015 April were performed in the 8-bit observing mode with 2-GHz bandwidth at all bands. The observations in 2015 September and 2016 January were performed in the 3-bit mode with 4-GHz bandwidth at C band, 6-GHz bandwidth at Ku band, and 8-GHz bandwidth at Ka band. Table 1 lists details for each observation.

For observations carried out prior to 2013 May, we reduced the data using `AIPS` (Greisen 2003). For observations carried out between 2013 May and 2016 May, we reduced the data using standard routines in `CASA` (McMullin et al. 2007).To obtain radio flux densities, we fit an elliptical Gaussian to the source image using `JMFIT` in `AIPS` and `gaussfit` in `CASA`. We estimated uncertainties in the flux density by adding in quadrature the uncertainty from the fit with a systematic uncertainty from absolute flux calibration. At frequencies above 10 GHz, we took the absolute flux density uncertainty to be 10%, and at frequencies below 10 GHz, we took the uncertainty introduced by the calibration to be 5%. During each observation of V809 Cep, we also observed the source J2339+6010 and source 3C48. Source J2339+6010 was used for complex gain calibration and source 3C48 was used for absolute flux calibration.

3 RESULTS

At radio frequencies above 13 GHz, roughly speaking, the flux density rose over the course of five to ten months, and then faded, but at frequencies below 7.4 GHz, V809 Cep brightened and faded twice (Fig. 1). On 2013 March 22 (day 48-Epoch 2), five weeks after a non-detection on 2013 February 14 (day 12-Epoch 1), the VLA detected V809 Cep at 7.4, 28.2, and 36.5 GHz. The source continued to brighten and was detected at all observed frequencies (4.6, 7.4, 28.2, and 36.5 GHz) on 2013 April 19. On day 76 (Epoch 4), the brightness at 4.6 GHz and 7.4 GHz reached local maxima, at flux densities of 0.41 ± 0.06 mJy and 0.63 ± 0.02 mJy, respectively (see Figure 1). We refer to this low frequency brightening two to three months after the initial outburst as the **early-time flare**. Even during the decay of the flare, the flux densities at high frequencies continued to rise and reached maxima between days 100 and 300 before beginning to decline (see Figure 1). Table 2 presents the flux densities and associated uncertainties. We take a measured flux density of between three and five times the total uncertainty to be a low-significance detection and a measured flux density of at least five times the total uncertainty to be a high-significance detection. Error bars correspond to 1σ uncertainties. V809 Cep appeared as an unresolved point source at all epochs.

The radio spectrum evolved through four distinct stages: 1) a broken power law during the rise of the early-time flare; 2) a simple power law between epochs 5 and 8 (Day 110 - 153), with a spectral index that remained stable at around $\alpha = 1.5$ to 1.6 for more than a month as the radio emission brightened again (taking $S_\nu \propto \nu^\alpha$, where S_ν is the flux density at frequency ν); 3) a broken power law again as the main decline started first at the highest and then lower frequencies; and 4) a simple, flat spectrum during the final decline. Over the full three-year time scale of the eruption – from 2013 March 22 (day 48) to 2016 January 28 (day 1090)– the radio spectrum evolved from one in which flux density increased with frequency, as expected for optically thick emitting material, to one in which flux density decreased slightly with frequency. We obtained the spectral index (α) for a given date and frequency range by performing a linear regression using `SciPy`'s least squares curve fitting method in log-log space, taking into account the uncertainties in the flux density mea-

Table 1. V809 Cep radio observations

Date	$t - t_0$[1]	MJD	Epoch	Configuration	Bands Observed	Time (min)[2]
02/14/2013	12	56337.0	1	D	C,Ka	47.9
03/22/2013	48	56373.5	2	D	C,Ka	47.9
04/04/2013	61	56386.9	3	D	C,Ka	47.9
04/19/2013	76	56401.6	4	D	C,Ka	29.9
05/23/2013	110	56435.4	5	C	C,U,Ka	29.9
06/10/2013	128	56453.5	6	C	C,U,Ka	29.9
06/16/2013	134	56459.3	7	C	C,U,Ka	29.9
07/05/2013	153	56478.3	8	C	C,U,Ka	29.9
08/27/2013	206	56531.2	9	C	C,U,Ka	29.9
09/27/2013	237	56562.2	10	B	C,U,Ka	29.2
11/22/2013	293	56618.0	11	B	C,U,Ka	29.9
11/30/2013	301	56626.8	12	B	C,U,Ka	29.9
12/16/2013	317	56642.8	13	B	C,U,Ka	29.9
03/14/2014	405	56719.7	14	A	C,U,Ka	29.9
04/29/2014	451	56776.5	15	A	C,U,Ka	30.2
05/28/2014	480	56805.6	16	A	C,U,Ka	30.2
07/08/2014	521	56846.3	17	D	C,U,Ka	29.9
09/06/2014	581	56906.2	18	D	C,U,Ka	29.9
11/07/2014	642	56968.0	19	C	C,U,Ka	29.9
01/29/2015	726	57051.1	20	B	C,U,Ka	27.4
04/21/2015	808	57133.5	21	B	C,U,Ka	29.9
09/06/2015	946	57271.4	22	A	Ka,U,S,C	31.4
01/28/2016	1090	57415.0	23	C	Ka,U,S,C	38.6

[1] We take the start time of the eruption, t_0, to be 2013 Feb 2.
[2] Total time on source

Table 2. V809 Cep radio flux densities measured with the VLA between 2013 Feb 14 to 2016 January 28, in mJy

Epoch	4.6 GHz	7.4 GHz	13.5 GHz	17.4 GHz	28.2 GHz	36.5 GHz
1	<0.051[1]	<0.018[1]	–	–	<0.031[1]	< 0.039 [1]
2	0.052 ± 0.016 [2]	0.189 ± 0.020	–	–	0.696 ± 0.040	0.718 ± 0.051
3	0.229 ± 0.027	0.503 ± 0.032	–	–	1.00 ± 0.028	0.926 ± 0.037
4	0.410 ± 0.061	0.627 ± 0.016	0.789 ± 0.015	0.942 ± 0.017	1.521 ± 0.031	2.143 ± 0.057
5	<0.054 [1]	0.334 ± 0.029	0.814 ± 0.025	1.150 ± 0.022	2.639 ± 0.065	3.809 ± 0.097
6	0.240 ± 0.027	0.434 ± 0.014	1.08 ± 0.015	1.56 ± 0.015	3.25 ± 0.039	4.69 ± 0.058
7	0.260 ± 0.033	0.542 ± 0.021	1.05 ± 0.017	1.48 ± 0.021	3.39 ± 0.0608	4.40 ± 0.082
8	0.252 ± 0.039	0.501 ± 0.015	1.366 ± 0.021	1.992 ± 0.024	4.228 ± 0.077	6.05 ± 0.12
9	0.287 ± 0.025	0.650 ± 0.024	1.583 ± 0.024	2.419 ± 0.035	3.33 ± 0.01	4.51 ± 0.03
10	0.292 ± 0.019	0.515 ± 0.030	1.494 ± 0.037	1.797 ± 0.089	3.40 ± 0.13	3.37 ± 0.12
11	0.448 ± 0.018	0.820 ± 0.013	1.98 ± 0.02	2.55 ± 0.02	3.79 ± 0.05	3.87 ± 0.07
12	0.417 ± 0.023	0.831 ± 0.015	1.88 ± 0.02	2.28 ± 0.02	3.19 ± 0.04	3.03 ± 0.05
13	0.380 ± 0.023	0.902 ± 0.016	2.04 ± 0.02	2.66 ± 0.02	3.72 ± 0.06	3.47 ± 0.08
14	0.492 ± 0.017	0.916 ± 0.012	1.697 ± 0.013	1.907 ± 0.017	2.314 ± 0.040	2.187 ± 0.065
15	0.513 ± 0.027	0.896 ± 0.014	1.34 ± 0.01	1.48 ± 0.02	1.55 ± 0.02 [5]	1.44 ± 0.03
16	0.495 ± 0.017	0.854 ± 0.011	1.22 ± 0.02	1.22 ± 0.02	1.26 ± 0.03 [5]	1.16 ± 0.03
17	0.458 ± 0.037	0.903 ± 0.029	1.09 ± 0.02	1.20 ± 0.03	1.20 ± 0.05	1.26 ± 0.08
18	0.526 ± 0.033	0.765 ± 0.024	0.904 ± 0.020	0.952 ± 0.025	0.980 ± 0.062	0.887 ± 0.072
19	0.492 ± 0.024	0.667 ± 0.014	0.713 ± 0.015	0.688 ± 0.017	0.697 ± 0.043	0.620 ± 0.051
20	0.437 ± 0.034	0.503 ± 0.022	0.515 ± 0.022	0.523 ± 0.022	0.456 ± 0.044	0.351 ± 0.062
21	0.413 ± 0.020	0.432 ± 0.015	0.402 ± 0.015	0.382 ± 0.018	0.458 ± 0.042	0.549 ± 0.057
22	0.265 ± 0.013 [3]	0.243 ± 0.012 [4]	0.288 ± 0.022	0.311 ± 0.032 [6]	0.234 ± 0.079 [5]	0.124 ± 0.071 [7]
23	0.305 ± 0.024 [3]	0.203 ± 0.014 [4]	0.176 ± 0.015	0.165 ± 0.011 [6]	0.191 ± 0.024 [5]	0.092 ± 0.025 [7]

[1] We take the threshold for detection to be a flux density of at least three times the uncertainty (3σ). We list non-detections as 2σ. upper limits.
[2] The flux density reported is measured at 4.7 GHz
[3] The flux density reported is measured at 5.0 GHz
[4] The flux density reported is measured at 7.0 GHz
[5] The flux density reported is measured at 16.5 GHz
[6] The flux density reported is measured at 29.5 GHz
[7] The flux density reported is measured at 35.0 GHz

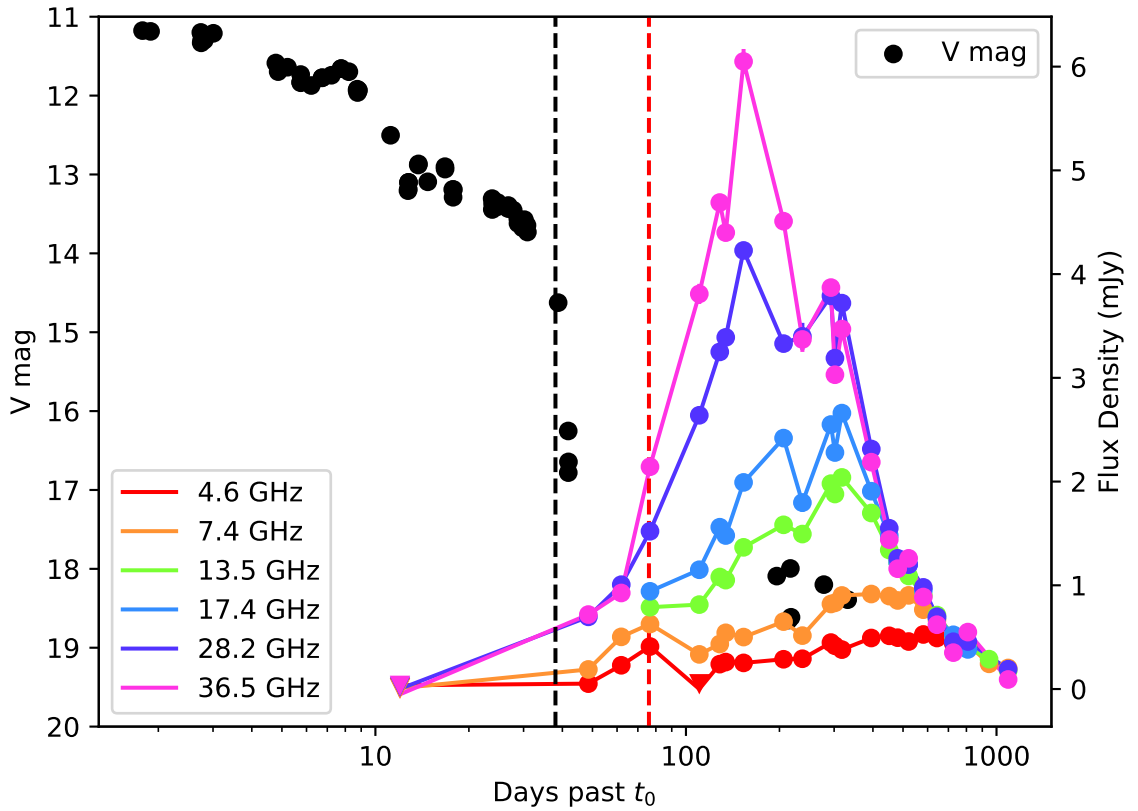


Figure 1. Optical and multi-frequency radio lightcurves of Nova V809 Cep as a function of days past discovery in the optical on 2013 February 2 (t_0). The triangles denote upper limits, and circles denote detections with significance of at least 3σ. The high-frequency radio lightcurves peak between day 100 and day 300 (Epochs 5-12), and there is a local maximum on day 76 (Epoch 4) at 4.6 and 7.3 GHz (red vertical line). Black points are V band magnitudes from (Munari et al. 2014). Error bars are smaller than the points. The vertical black line denotes the onset of dust formation on day 37.

surements. We generally split the frequencies into low frequencies (4.6, 7.4 GHz), intermediate frequencies (13.5 GHz, 17.4 GHz), and high frequencies (28.2, 36.5 GHz). If the spectral indices at low, intermediate, and high frequencies were within 0.2 of each other, we fit them with a single powerlaw. If the spectral indices differed by more than 0.2, we fit the spectrum with a broken powerlaw.

Figure 2 shows the radio spectral energy distribution for selected epochs between 2013 March 22 and 2016 January 28. During Epochs 2, 3, and 4 (stage 1), the spectral index at low frequencies (4.6 GHz and 7.4 GHz) differed from that at high frequencies. At low frequencies, the spectral index evolved from $\alpha = 2.8 \pm 0.7$ in Epoch 2 to a much flatter $\alpha = 0.48 \pm 0.07$ in Epoch 4. In contrast, at high frequencies the spectral index evolved from being quite flat at Epoch 2 ($\alpha = 0.1 \pm 0.4$) to rising with $\alpha = 1.5 \pm 0.2$ at Epoch 4. During stage 3 (Epochs 10-16), the spectrum flattened first at the highest frequencies (Epoch 10) and subsequently at lower frequencies, leading to stage 4 (Epochs 18-22), during which time the spectrum was flat ($\alpha = 0.1 \pm 0.1$ at Epoch 22) across the full range of frequencies.

4 DISCUSSION

4.1 Early Time Radio Flare

During the second and third month of the outburst, the nova produced a flare of low-frequency radio emission that brightened more quickly than expected for freely expanding thermal ejecta and reached a brightness that exceeded expectations for thermally emitting material expanding at the speed of the principal optical absorbing system, suggesting that the flare was non-thermal in origin. The first piece of evidence in support of non-thermal emission is the rapid brightening at low frequencies. Between Epochs 2 and 3, the 4.6-GHz emission increased roughly as t^6, where t here is the time since t_0. Even if the material that generated the early-time flare was not ejected from the region of the white dwarf until four days after the start of the eruption (Munari et al. 2014), the 4.6-GHz flux density increased faster than t^4. During the same interval, the 7.4-GHz brightness increased as t^4. Between Epochs 3 and 4, the 4.6-GHz emission continued to increase faster than t^2. For a freely expanding blackbody with constant temperature, the brightness of thermal radio emission can only increase as fast as t^2, proportional to the increasing area of the source on the sky. Although it would be possible for the size of a thermally emitting source to increase faster than t^2 if an ionization front was rapidly propagating through the ejecta, or if the electron temperature of the emitting material was increasing, the high radio brightness during Epochs 3 and 4 (see discussion below and Fig. 3) disfavors either of these possibilities.

The second piece of evidence in support of non-thermal emission is the strength of the low-frequency radio emission during Epochs 3 and 4. We parameterize the radio flux density in terms of a *brightness temperature,* T_b – the minimum electron temperature required for the observed radio emission to arise from thermal Bremsstrahlung. Brightness temperature is a measure of sur-

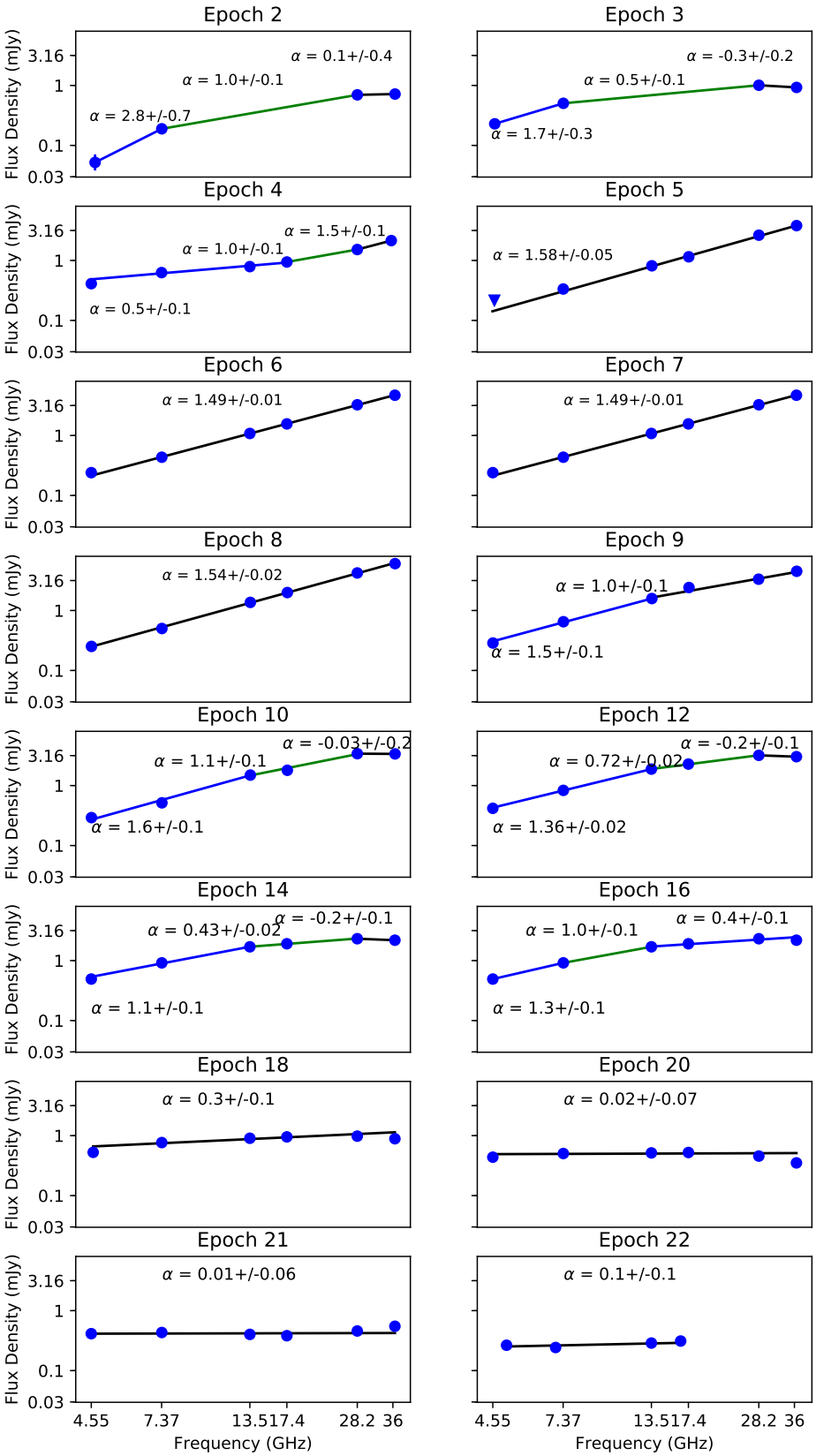


Figure 2. Evolution of the spectral energy distribution of V809 Cep for selected epochs between Epoch 1–23. Upper limits are plotted as triangles, and error-bars are typically smaller than the points. α represents the spectral index. The peak of the early-time flare occurred at Epoch 4.

face brightness. If a uniform temperature, Bremsstrahlung-emitting medium is optically thick over its full area on the sky, the brightness temperature corresponds to its physical temperature; however, if it is even partially optically thin, or if the radio emission emanates from a region that is smaller than the size of the putative spherical ejecta, then the brightness temperature only provides a lower limit for the physical temperature. Assuming a spherically expanding shell, T_b is given by:

$$T_b(\nu, t) = \frac{S_\nu(t) c^2 D^2}{2\pi k_b \nu^2 (v_{ej} t)^2}, \quad (1)$$

where c is the speed of light, k_b is the Boltzmann constant, t is the time since t_0, and v_{ej} is the maximum expansion velocity. Using a distance of D = 6.5 kpc and a maximum ejection velocity of 1200 km/s (corresponding roughly to the faster of the two principal absorption systems seen in optical spectroscopy; Munari et al. 2014), the brightness temperature at 4.6 GHz reached $1.3 \pm 0.2 \times 10^5$ K (Epoch 4 (day 76); see Figure 3). For the early-time radio flare to have had a thermal origin would therefore require that on day 76 (Epoch 4), the ejecta included a shell of material with an electron temperature of at least 10^5 K, that was at least as extended on the sky as the 1200 km/s flow, and that was dense enough to be optically thick at 4.6 GHz. If the radio emission emanated from knots, or a portion of the ejecta that subtended a smaller solid angle on the sky than the 1200 km/s flow, the required electron temperature for the early-time flare to have been thermal is even higher. We argue below that such a large, hot, dense ejecta on day 76 (Epoch 4) seems unlikely.

Crucially, given that $T \sim 10^4$ K is the approximate equilibrium temperature for a plasma cooled by forbidden emission lines (Weston et al. 2016a), photoionized ejecta from novae are typically expected to have electron temperatures of around this value. In fact, Cunningham et al. (2015) found that for a wide range of white dwarf masses, ejecta masses, and ejecta speeds, the temperature of the photoionized ejecta generally does not exceed a few times 10^4 K at any point. It is possible that the peak brightness of the early-time radio flare in V809 Cep could have been generated by the most spatially extended flow associated with the so-called diffuse enhanced optical spectroscopic system (which had speeds of up to 2000 km/s, Munari et al. 2014) if it had a temperature of 4×10^4 K and was completely optically thick. However, the low-frequency spectral index on day 76 (Epoch 4) was $\alpha = 0.5 \pm 0.1$, much lower than the $\alpha \approx 2$ expected for optically thick Bremsstrahlung, indicating that the radio-emitting ejecta were *not* optically thick at that time.

The expected temperature for photoionized ejecta and the $\alpha = 0.5$ spectral index thus both argue against a thermal origin for the early-time flare.

The high T_b is also unlikely to be due to a shell of shock-heated, 10^5 K gas between the forward and reverse shocks. Steinberg & Metzger (2018) explore the possibility of forward and reverse shocks in the ejecta producing a shell of cool ($\sim 10^4 K$), dense gas bounded by a shell of $T \sim 10^6$ K gas. We define $M_{hot,needed}$ as the mass of 10^5 K gas that would be needed to make a shell of width L_{cool} optically thick at radio frequencies and $M_{hot,expected}$ as the mass of 10^5 K gas theoretically expected to be present. Below, we compare $M_{hot,expected}$ and $M_{hot,needed}$.

The expected geometrical thickness of the shell of hot gas can be approximated as the cooling length (L_{cool}; Steinberg & Metzger 2018):

$$L_{cool} = v_{shock} t_{cool}/4. \quad (2)$$

Because it is not clear whether the early-time radio flare was the result of the forward or reverse shock, we take v_{shock} to be the velocity of the forward shock. The reverse shock was directed into the fast moving, low density ejecta and thus had a higher velocity than the forward shock which was directed into higher density ejecta. This lower forward-shock velocity ends up being a more conservative estimate for v_{shock} (see Fig. 4 for a comparison between $M_{hot,needed}$ and $M_{hot,expected}$ as a function of v_{shock}). The maximum velocity of the principle absorption system seen in optical spectroscopy was 1200 km/s, and the lowest expansion velocity observed was 600 km/s (Munari et al. 2014); therefore, we assume a shock velocity between 600 km/s and 1200 km/s. As gas behind the shock cools radiatively, t_{cool} is given by (Steinberg & Metzger 2018):

$$t_{cool} = \frac{\bar{\mu}(3/2) k_b T_{shock}}{\mu_p \mu_e n_{shock} \Lambda}, \quad (3)$$

where the mean molecular weight is $\bar{\mu} = 0.74$ for a typical composition of a fully ionized classical nova ejecta (Vlasov et al. 2016; Sokolovsky et al. 2020, $\mu_p = 1.39$, and $\mu_e = 1.16$. From Steinberg & Metzger (2018), we estimate the value of the cooling function (Λ) for 10^5 K gas to be 10^{-20} cm^3/s. Assuming $\bar{\mu} = 0.74$, the temperature of the shock, T_{shock}, is related to the shock velocity as (Steinberg & Metzger 2018):

$$T_{shock} \approx 1.4 \times 10^7 \text{ K} \left(\frac{v_{shock}}{10^3 \text{ km s}^{-1}} \right)^2. \quad (4)$$

Multiplying the mean molecular weight by the expected shell thickness and number density at the location of the shell on day 76 – for the appropriate range of shock velocities, a $1/r^2$ density profile (where r is the distance from the white dwarf), a number density (n_{shock}) at $R_{shock} = v_{shock} t$ from the standard shock jump conditions (Steinberg & Metzger 2018) $n_{shock} = 4n$, and a total ejecta mass determined from the late-time radio evolution – we find that $M_{hot,expected}$ likely fell between 10^{-10} and $10^{-8} M_\odot$ (see Fig. 4).

For the early-time flare to have been due to thermal emission from gas enclosed within L_{cool}, that gas must either have been optically thick with a temperature in excess of $T_b = 1.3 \times 10^5$ K or had an even higher temperature. In fact, the mass of hot gas that would have been needed to make the hot shell optically thick, $M_{hot,needed}$, is more than an order of magnitude greater than $M_{hot,expected}$. To estimate $M_{hot,needed}$, we assume the hot shell expanded with velocity v_{shock}. We derive the number density of electrons needed to make a $T_e \sim 10^5$ K shell optically thick at 4.55 GHz by setting $\tau_\nu = 1$ in the expression for the emission measure and taking a constant density profile within the hot shell. The emission measure is $EM = \int_{r_o}^{r_i} n_e^2 dl$, where n_e is the electron density. Following Bode & Evans (2008), we calculate the emission measure needed to make the hot shell optically thick ($\tau_\nu = 1$) from:

$$\tau_\nu = 1 = 8.235 \times 10^{-2} \left(\frac{T_e}{K} \right)^{-1.35} \left(\frac{\nu}{GHz} \right)^{-2.1} \frac{EM(\tau_\nu)}{cm^{-6} pc}. \quad (5)$$

Figure. 4 shows both $M_{hot,expected}$ and $M_{hot,needed}$ enclosed in a shell of thickness L_{cool} as a function of of shock velocity.

For v_{shock} between 600 km/s to 1200km/s, $M_{hot,needed}$ exceeded $M_{hot,expected}$ by at least an order of magnitude. For v_{shock} of 900km/s, $M_{hot,needed} = 1.5x10^{-8} M_\odot$ and $M_{hot,expected} = 8.5x10^{-10} M_\odot$. It is thus implausible for the high brightness temperature to have been the result of thermal emission from a shock-heated shell. This finding further supports our assertion that the high brightness temperature is most likely the result of non-thermal emission produced in a shock.

Non-thermal emission from novae is widely accepted to be the result of internal shocks in the ejecta (Chomiuk et al. 2020a; Vlasov et al. 2016; Finzell et al. 2018; Weston et al. 2016a; Franckowiak

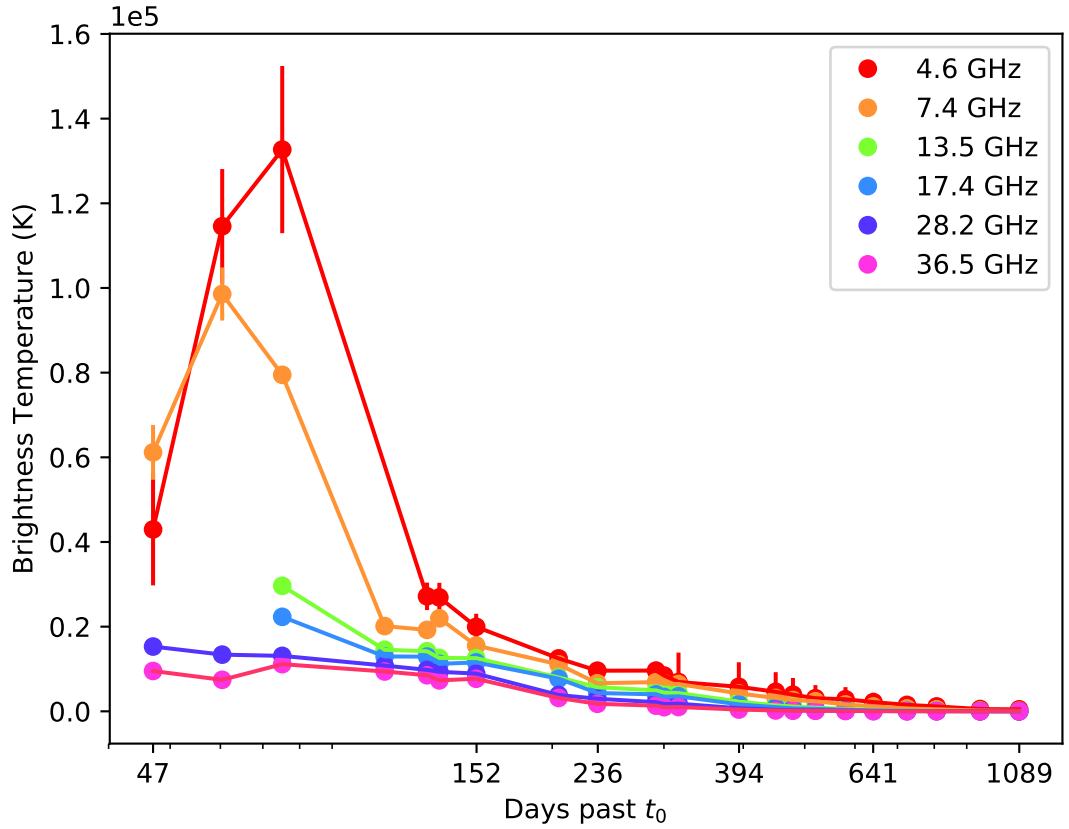


Figure 3. Brightness temperature as a function of time for each of the frequencies at which VLA observed V809 Cep using D=6.5kpc and source size described in text. The high brightness temperature in the first three months after eruption constitutes possible evidence for non-thermal emission and shocks

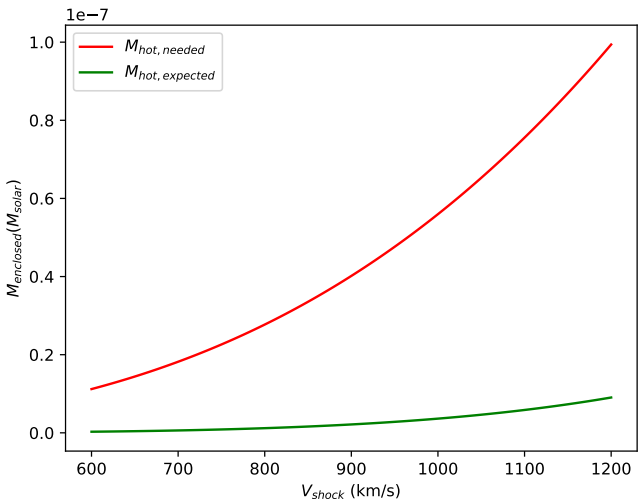


Figure 4. The mass expected in the 10^5 K hot shell between the shocks ($M_{hot,expected}$) and the hot-shell mass needed to explain the early-time flare with just thermal emission ($M_{hot,needed}$) for a range of shock velocities from 600 km s^{-1} to 1200 km s^{-1}.

et al. 2018; O'Brien & Lloyd 1994). The collision of the fast and slow flows results in shocks that are responsible for accelerating particles to relativistic speeds. Novae V1723 Aql (Weston et al. 2016a), V5589 Sgr (Weston et al. 2016b) and Nova 1324 Sco (Finzell et al. 2018) had brightness temperatures of greater than 10^5 K, interpreted as evidence for radio synchrotron emission from shocks. We similarly propose that the bright radio emission that the VLA detected on April 19 2013 (Epoch 4) was the result of shocks in ejecta from V809 Cep. V809 Cep thus joins six other classical novae with radio evidence for shocks: V906 Car (Aydi et al. 2020a), V1324 Sco (Finzell et al. 2018), V1723 Aql (Weston et al. 2016a), 5589 Sgr (Weston et al. 2016b), V959 Mon (Chomiuk et al. 2014a) and QU Vul (Taylor et al. 1987). Non-thermal radio emission has also been found in the eruptions of closely related objects including the helium nova V445 Pup (Nyamai et al. 2021) and the symbiotic system V407 Cyg (Giroletti et al. 2020).

4.2 Spectral Evolution

The radio spectral evolution during the rise to maximum of the early-time flare in V809 Cep had some resemblance to theoretical predictions for synchrotron from internal shocks in novae by Vlasov et al. (2016). Those authors suggested that photo-ionized gas ahead of the shock initially absorbs radio synchrotron emission, causing the spectral index (α) to evolve from approximately 2.0, as expected for optically thick thermal emission, to 2.5 when the photo-ionized gas ahead of the shock becomes transparent and optically thick synchrotron emission begins to dominate the spectrum. Vlasov et al. (2016) predicted that the spectral index then gradually decreases toward the $\alpha = -0.7$ expected for optically thin synchrotron (the exact

value depends on the energy spectrum of the emitting particles, e.g. Pacholczyk 1970). Later, the spectral index is expected to once again rise as the radio emission becomes dominated by optically thick thermal emission from the bulk of the expanding, photoionized ejecta. The peak of the early-time flare occurs as the synchrotron transitions from optically thick to optically thin (Vlasov et al. 2016).

At low frequencies (below 7.4 GHz), the radio emission during the early-time flare in V809 Cep was consistent with theoretical expectations – if the VLA began detecting the flare when photoionized gas ahead of the shock had already become partially transparent. During the flare, the low-frequency spectral index transitioned from a high value suggestive of optically thick synchrotron emission (2.8 ± 0.7 in Epoch 2) to the more modest value of 0.5 ± 0.1 at the peak of the flare (during Epoch 4). Though the error bars on the low frequency spectral index at Epoch 2 are large, in combination with the high brightness temperature, the high spectral index implies optically thick synchroton emission.

The flattening of the low-frequency spectral index at Epoch 4 suggests that the spectrum was indeed transitioning from one indicative of optically thick to optically thin synchrotron emission at that time, as predicted by Vlasov et al. (2016). At Epoch 5, the low-frequency spectral index increased again, to 1.58 ± 0.05, as expected for optically thick thermal emission from the main, expanding ejecta beginning to dominate over the early-time synchrotron emission.

At high frequencies, the radio emission during the early-time flare can also be understood within the framework of Vlasov et al. (2016). Synchrotron emission from an expanding medium is expected to become optically thin, and the spectral index to decrease, at the highest frequencies first (29 GHz and above, in our case). The high-frequency spectral indices at Epochs 2 and 3 of 0.1 ± 0.4 and -0.3 ± 0.2, respectively, thus follow the spectral evolution modeled in Vlasov et al. (2016) if the synchrotron emission had already become fairly optically thin at those frequencies by Epochs 2 and 3. Moreover, because the high-frequency radio spectrum was already quite flat when the VLA first detected the source in Epoch 2, with the high-frequency flux densities well below an extrapolation of the low-frequency spectrum at that time, synchrotron emission at frequencies higher than 7.4 GHz likely peaked before it peaked at low frequencies, and even prior to the first radio detection. Further supporting the possibility that any synchrotron peaked at high frequencies before low frequencies, at 7.4 GHz, the brightness temperature peaked during Epoch 3, an epoch before the peak at 4.6 GHz. Brightness temperature represents a lower limit on the physical temperature of an optically thin gas; therefore, we expect the brightness temperature to peak at high frequencies prior to peaking at low frequencies as the high frequencies become optically thin first. Figure 3 displays a peak first a Epoch 3 (Day 61) at 7.4 GHz and later at Epoch 4 (Day 76) at 4.6 GHz. We thus posit that the early-time flare peaked at high frequencies prior to the first radio detection.

Absorption by photo-ionized gas ahead of the shock would initially obscure the non-thermal emission and produce a delay between the early-time radio maxima at progressively lower frequencies (Vlasov et al. 2016). As the photo-ionized gas ahead of the shock begins to diffuse and become optically thin at lower frequencies, the non-thermal emission from the shock becomes increasingly dominant first at higher frequencies and finally at lower frequencies. So, hints that the synchrotron flare peaked at higher frequencies first (rather than at all frequencies simultaneously) suggest that non-thermal emission from internal shocks in the V809 Cep ejecta was initially absorbed by photo-ionized gas ahead of the shock. However, even if any synchrotron emission was initially somewhat absorbed by photoionized gas, the high spectral index of 2.8 ± 0.7 during Epoch 2 (Day 48) would indicate that we caught the flare when the putative synchrotron emission was already peeking through at low frequencies.

The radio spectral evolution during Stage 2 (Epochs 5-9) further supports our assertion that the spectrum during stage 1 was attributable to an emission component that was physically distinct from the main photoionized ejecta. As the early emission component thinned, the radio spectrum became increasingly dominated by optically thick thermal emission. Indeed, during Epochs 4 (Day 76), the spectral index at high frequencies rose to 1.5 ± 0.1, indicative of optically thick thermal emission. During Epoch 5 through 9 (Day 110 - 206) , the spectral index for all frequencies increased to 1.58 ± 0.05 and remained around 1.5 as the ejecta expanded and the radio emission brightened for the remainder of stage 2. Although the stage 2 spectral indices were lower than the expected 2.0 for optically thick thermal emission from a medium with an infinitely sharp outer edge, values of 1.5 are typical for actual nova remnants. Therefore, the radio spectral evolution was consistent with emission from an increasingly optically thin synchrotron source and a gradually brightening optically thick thermal component. During stage 3 and 4, the radio spectrum was typical of a thermal source becoming increasingly optically thin, with the spectrum flattening at progressively lower frequencies as gas began to become optically thin first at high frequencies (> 29 GHz) and by Epoch 20 (Day 726) at all frequencies.

Table 3: V809 Cep timeline

Event	Date	$t - t_0$
Optical Detection	2013 February 2	0
Optical Peak	2013 February 3	1
Onset of dust production	2013 March 11	37
Synchrotron detected	2013 March 22	48
Peak of Low-Frequency synchrotron	2013 April 19	76

4.3 Quasi-simultaneity of synchrotron flare and dust formation

Around the start of the early-time flare, dust production also commenced, providing evidence for a connection between shocks and dust formation. In the shock-dust model (Derdzinski et al. 2017), internal shocks in the ejecta lead to dust condensation. We would naively expect, therefore, to see evidence for the shocks *prior* to the onset of dust formation, which began around 2013 March 11 (day 37; Munari et al. 2014). The VLA did not observe V809 Cep between day 12 (Epoch 1) and day 48 (Epoch 2) of the eruption, so we cannot pinpoint the exact time at which synchrotron emission appeared (or peaked at high frequencies). But on day 48 (Epoch 2), 11 days past the onset of dust formation, we detected radio emission almost certainly associated with shocks within the ejecta. Therefore, both signatures of shocks and dust appeared during the one month gap between Epoch 1 (Day 12) and Epoch 2 (Day 48). Given the evidence that the early-time flare did not peak at the same time at all frequencies and therefore that any synchrotron was initially obscured, the radio observations are consistent with the shocks arising either slightly before or around the same time as the onset of dust production.

4.4 Properties of the Thermal Ejecta

Starting about nine months into the eruption, the radio emission was reasonably consistent with Bremsstrahlung (free-free emission) from freely expanding, photoionized ejecta. We modeled the main ejecta as a Hubble-flow (Gehrz 2008; Finzell et al. 2018; Weston et al. 2016a; Seaquist & Palimaka 1977; Hjellming et al. 1979), in which the ejecta consists of a homologously expanding isothermal spherical shell of gas bound between inner and outer radii r_{inner} and r_{outer}, with a r^{-2} density profile (where r is the distance from the white dwarf), and a volume filling factor, f. The filling factor is a measure of inhomogeneities in the ejecta, such as clumps (e.g., Weston et al. 2016a; Hjellming 1996). We assume no inhomogeneities ($f = 1$). If the ejecta were actually clumpy, that would reduce the ejecta mass needed to generate the observed radio emission (Weston et al. 2016a; Hjellming 1996; Abbott et al. 1981; Leitherer & Robert 1991; Chomiuk et al. 2014b).

At low frequencies (< 7.4 GHz) during the first six or so months of the outburst, the model fit the observed flux densities poorly, and as expected, was unable to account for the early-time flare. At 13.5 and 17.0 GHz, the discrepancy between the model and the observed flux densities during the first few months of the eruption supports our contention (in Sec. 4.2) that the flare at these frequencies could have peaked before Epoch 4 (Day 76). At these frequencies, the Hubble-Flow model matched the observed flux densities well after Epoch 4 (Day 76). At Epoch 4 (Day 76), however, the observed flux density at 17.4 GHz was 0.94±0.02 mJy, 0.61 mJy in excess of the the model flux density of 0.33 mJy. At 13.5 GHz, the observed flux density was 0.789 ± 0.002, 0.58 mJy in excess of the model flux density. That the observed 13.5- and 17.4-GHz flux densities were far in excess of the model during Epoch 4 (Day 76) indicates that any synchrotron emission was still dominant at those frequencies at that time and could therefore have peaked even earlier (the VLA did not collect data at these frequencies during Epochs 2 and 3 (Day 48 and Day 61)).

At 28.8 and 36.5 GHz, and after approximately days 200-300 (¿Epoch 9) at all frequencies, however, the model reproduces the observed flux densities moderately well. Using $D = 6.5$ kpc, $v_{ej} = 1200$ km s^{-1}, and $v_{min} = 600$ km s^{-1}, we determined the best-fit ejecta mass and temperature by employing the Markov Chain Monte Carlo program pymc. We found $M_{ejected} = (1.1 \pm 0.1) \times 10^{-4} M_{\odot}$ and $T = (0.8 \pm 0.2) \times 10^4 K$ when the hubble flow model was fit to the reduced flux densities starting from Epoch 2 (Day 48) (first detection). Figure 5 displays the observed flux densities as well as the modeled free-free emission for $D = 6.5$ kpc, $M_{ejected} = (1.1 \pm 0.1) \times 10^{-4} M_{\odot}$ and $T = (0.8 \pm 0.2) \times 10^4$ K.

5 CONCLUSIONS

- The radio light-curves at 4.6 GHz and 7.4 GHz display an early-time flare that peaks at Epoch 4 (day 76). At 4.6 GHz, the brightness temperature at that time was at least $1.5 \times 10^5 K$.
- At low frequencies (< 7.4 GHz) the rise of the early-time flare began at Epoch 2 (Day 48, 2013 March 22). The spectral index at low frequencies at Epoch 2 (Day 48) was 2.82 ± 0.71.
- The high brightness temperature at the peak of the early-time flare at Epoch 4 (Day 76) combined with the high spectral index at Epoch 2 (Day 48) suggests the presence of non-thermal emission due to internal shocks in the nova ejecta. This is the first report showing evidence for shocks in V809 Cep.
- The discovery of non-thermal radio emission early in the evolution of the eruption puts V809 Cep in the same category as six other novae known to show radio evidence for shocks: V906 Car (Aydi et al. 2020a), V1324 Sco (Finzell et al. 2018), V1723 Aql (Weston et al. 2016a), V5589 Sgr (Weston et al. 2016b), V959 Mon (Chomiuk et al. 2014a),and QU Vul (Taylor et al. 1987).
- At late times (after Epoch 4 (Day 76)), the radio emission was consistent with thermal emission from freely expanding ejecta with a maximum ejecta speed of 1200km/s, v_{min} = 600km/s, D =6.5 kpc, $T = 0.8 \times 10^4 \times 10^4 K$, and a $M_{ejected} = 1.1 \times 10^{-4} M_{\odot}$.
- Our finding that a radio synchrotron flare associated with internal shocks in the ejecta began during a roughly month-long period of time during which dust formation also commenced supports the idea that shocks could form ideal environments for dust formation around novae.
- If shocks in the nova ejecta lead to dust formation, the 11 day delay between the onset of dust and the rise of the early-time flare suggests that the radio emission was absorbed by photo-ionized gas ahead of the shock.

DATA AVAILABILITY

The data underlying this article will be shared on reasonable request to the corresponding author. The uncalibrated radio observations are publicly available from the NRAO Data Archive (archive.nrao.edu or data.nrao.edu)

ACKNOWLEDGEMENTS

The National Radio Astronomy Observatory is a facility of the National Science Foundation operated under cooperative agreement by Associated Universities, Inc. A. B. and J. L. S. acknowledge support from NSF grant AST-1816100 and Heising-Simons Foundation grant 2017-246, as well as NRAO 362918. Laura Chomiuk, Adam Kawash, Elias Aydi, and Kirill V. Sokolovsky were supported by NSF grant AST-1751874 and a Cottrell fellowship of the Research Corporation.

REFERENCES

Abbott D. C., Bieging J. H., Churchwell E., 1981, ApJ, 250, 645
Ackermann M., et al., 2014, Science, 345, 554
Atwood W. B., et al., 2009, ApJ, 697, 1071
Aydi E., et al., 2020a, Nature Astronomy, 4, 776
Aydi E., et al., 2020b, ApJ, 905, 62
Blandford R. D., 1994, ApJS, 90, 515
Bode M. F., Evans A., 2008, Classical Novae
Brand J., Blitz L., 1993, A&A, 275, 67
Buson S., Jean P., Cheung C. C., 2019, The Astronomer's Telegram, 13114, 1
Chomiuk L., et al., 2014a, Nature, 514, 339
Chomiuk L., et al., 2014b, ApJ, 788, 130
Chomiuk L., Metzger B. D., Shen K. J., 2020a, arXiv e-prints, p. arXiv:2011.08751
Chomiuk L., Metzger B. D., Shen K. J., 2020b, arXiv e-prints, p. arXiv:2011.08751
Cunningham T., Wolf W. M., Bildsten L., 2015, ApJ, 803, 76
Della Valle M., Izzo L., 2020, A&ARv, 28, 3
Derdzinski A. M., Metzger B. D., Lazzati D., 2017, MNRAS, 469, 1314
Downes R. A., Duerbeck H. W., 2000, AJ, 120, 2007
Evans A., 2001, Ap&SS, 275, 131
Finzell T., et al., 2018, ApJ, 852, 108
Franckowiak A., Jean P., Wood M., Cheung C. C., Buson S., 2018, A&A, 609, A120

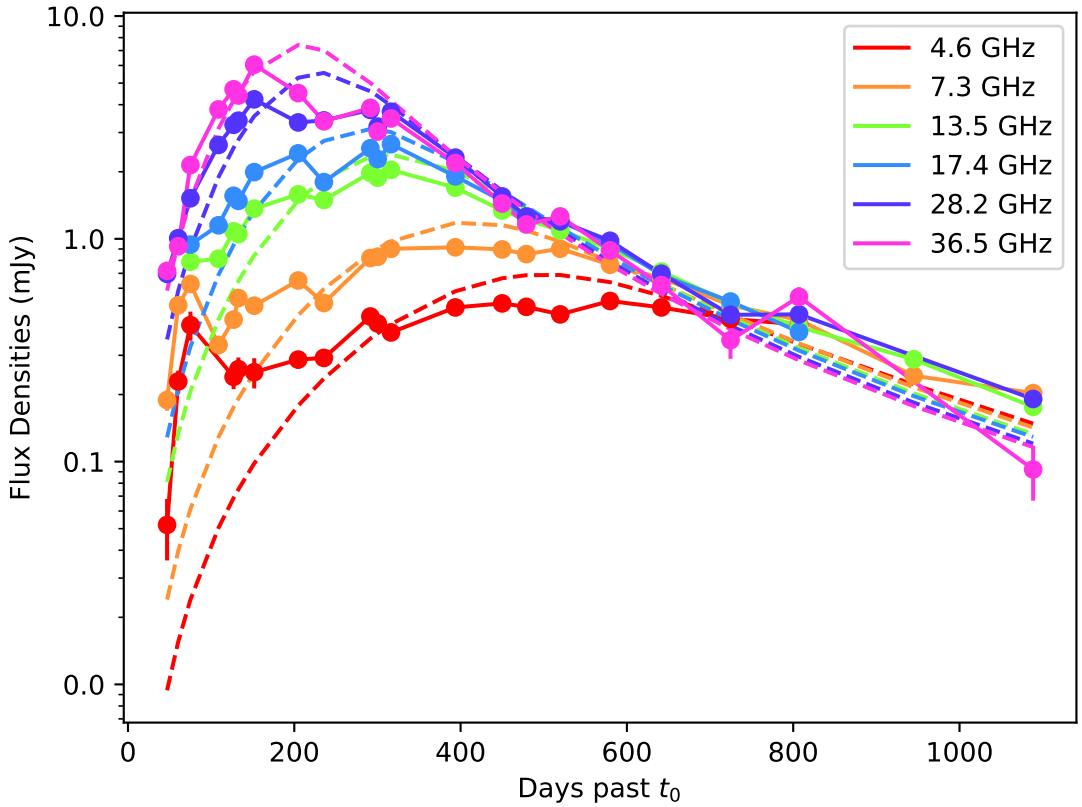


Figure 5. Hubble Flow model compared with observed flux densities. The dashed lines show the model flux densities, and the solid points denote the observed flux densities. The model fluxes are calculated using $M_{ejected} = 1.1 \times 10^{-4} M_{\odot}$, $T = 0.8 \times 10^{4} K$, v_{ej} = 1200 km/s,v_{min}=600km/s, and D = 6.5 kpc

Gallagher J. S., 1977, AJ, 82, 209

Gehrz R. D., 2008, Infrared studies of classical novae, 2 edn. Cambridge University Press, p. 167–193, doi:10.1017/CBO9780511536168.010

Giroletti M., et al., 2020, A&A, 638, A130

Greisen E. W., 2003, AIPS, the VLA, and the VLBA. p. 109, doi:10.1007/0-306-48080-8˙7

Hjellming R. M., 1996, in Taylor A. R., Paredes J. M., eds, Astronomical Society of the Pacific Conference Series Vol. 93, Radio Emission from the Stars and the Sun. p. 174

Hjellming R. M., Wade C. M., Vandenberg N. R., Newell R. T., 1979, AJ, 84, 1619

Leitherer C., Robert C., 1991, ApJ, 377, 629

Li K.-L., et al., 2017, Nature Astronomy, 1, 697

Martin P., Dubus G., Jean P., Tatischeff V., Dosne C., 2018, A&A, 612, A38

McMullin J. P., Waters B., Schiebel D., Young W., Golap K., 2007, in Shaw R. A., Hill F., Bell D. J., eds, Astronomical Society of the Pacific Conference Series Vol. 376, Astronomical Data Analysis Software and Systems XVI. p. 127

Metzger B. D., Finzell T., Vurm I., Hascoët R., Beloborodov A. M., Chomiuk L., 2015, MNRAS, 450, 2739

Metzger B. D., Caprioli D., Vurm I., Beloborodov A. M., Bartos I., Vlasov A., 2016, MNRAS, 457, 1786

Munari U., et al., 2014, MNRAS, 440, 3402

Nyamai M. M., Chomiuk L., Ribeiro V. A. R. M., Woudt P. A., Strader J., Sokolovsky K. V., 2021, MNRAS, 501, 1394

O'Brien T. J., Lloyd H. M., 1994, Ap&SS, 216, 167

Pacholczyk A. G., 1970, Radio astrophysics. Nonthermal processes in galactic and extragalactic sources

Seaquist E. R., Palimaka J., 1977, ApJ, 217, 781

Shore S. N., Kuin N. P., Mason E., De Gennaro Aquino I., 2018, A&A, 619, A104

Sokolovsky K. V., et al., 2020, MNRAS, 497, 2569

Starrfield S., Iliadis C., Hix W. R., 2016, PASP, 128, 051001

Steinberg E., Metzger B. D., 2018, MNRAS, 479, 687

Strope R. J., Schaefer B. E., Henden A. A., 2010, AJ, 140, 34

Taylor A. R., Seaquist E. R., Hollis J. M., Pottasch S. R., 1987, A&A, 183, 38

Vlasov A., Vurm I., Metzger B. D., 2016, MNRAS, 463, 394

Weston J. H. S., et al., 2016a, MNRAS, 457, 887

Weston J. H. S., et al., 2016b, MNRAS, 460, 2687